J Geophys (1986) 59:149-156

Journal of Geophysics

Original investigations

Complete seismogram synthesis for transversely isotropic media

B. Mandal and B.J. Mitchell

Department of Earth and Atmospheric Sciences, Saint Louis University, P.O. 8099, Laclede Station, Saint Louis, MO 63156, USA

Abstract. The response at the surface of a layered transversely isotropic medium due to a buried dislocation source can be expressed by using propagator matrices and discrete wavenumber summation. These operations produce complete seismograms for earth-quake or explosion sources which include all body- and surface-wave phases for this specialized anisotropic structure. In order to test the numerical procedures, synthetic seismograms at near distances for an isotropic model are compared with those generated by other methods. The agreement is found to be satisfactory in all cases. Comparisons of synthetic seismograms for anisotropic models having a small degree of anisotropy with similar but isotropic models, show that significant differences in travel times, amplitudes and wave forms can be caused by the anisotropy.

Key words: Anisotropy – Transverse isotropy – Propagator matrices – Wavenumber summation – Synthetic seismogram

Introduction

In recent years, increasing numbers of observational studies have required interpretations in terms of anisotropic elastic properties. These have included regional studies (e.g. Schlue and Knopoff, 1977; Yu and Mitchell, 1979; Cara et al., 1980) and global studies (e.g. Anderson and Dziewonski, 1982; Tanimoto and Anderson, 1984) of seismic surface waves, observations of azimuthal variations of body-wave velocities (e.g. Bamford and Crampin, 1977; Kogan, 1984) and observations of shear-wave splitting (e.g. Bezgodkov and Yegorkina, 1984). These and other studies have provided strong support for the existence of wide-spread anisotropy with consistent orientation in at least some regions of the earth as first proposed by Hess (1964). Such anisotropy may be caused by a variety of mechanisms including preferred crystal orientation, aligned cracks and rheological alignments.

The theoretical formulation required for computing surface-wave velocities in stratified anisotropic media which is transversely isotropic with a vertical axis of symmetry was developed by Anderson (1961) and Harkrider and Anderson (1962), and in general anisotropic media by Crampin (1970) and Crampin and Taylor (1971). It has also been possible to compute synthetic seismograms for body waves in general anisotropic media (Keith and Crampin, 1977). Synthesis schemes have also been developed for general anisotropy in stratified media (Booth and Crampin, 1983; Fryer and Frazer, 1984) by using Kennett's (1974) reflectivity approach.

This study presents a method for computing complete seismograms, which include all phases which traverse an anisotropic medium which is transversely isotropic with a vertical axis of symmetry. This type of anisotropy has been observed in some sediments (Robertson and Corigan, 1983) and may be expected to occur in planar igneous bodies or floating ice-sheets. It has also been proposed that this type of anisotropy occurs in the asthenosphere (Schlue and Knopoff, 1977) where molten inclusions have been modeled as flat, penny-shaped cracks.

We begin by using expressions from Takeuchi and Saito (1972) for surface-wave displacements and stresses in cylindrical coordinates. Those equations are based on an earlier formulation by Alterman et al. (1959). In the present paper we assume that the earth is composed of transversely isotropic layers overlying a half-space which may also be transversely isotropic. We compute the response of the medium to a point dislocation source using propagator matrices (Gilbert and Backus, 1966) and discrete wavenumber integration (Bouchon, 1981). We verify our computations of ground motion time history by comparing results for an isotropic model with results obtained using existing methods.

Theory

We define our model as $N-1$ homogeneous, anisotropic (transversely isotropic with vertical axis of symmetry) or isotropic layers overlying a half-space. With this symmetry, each anisotropic layer is characterized by five elastic constants A, C, L, N, F as defined by Love (1927, p. 160) and density ρ. A and C are related to dilatational wave velocity and L and N to shear wave velocity. Three kinds of plane waves corresponding to P, SV, and SH waves in isotropic media can be transmitted independently (Matuzawa, 1943). The velocities of such waves are as follows, for horizontal trans-

Offprint requests to: B.J. Mitchell

mission:

$$
\begin{aligned}
\frac{A}{\rho} &= \alpha_H^2 \quad \text{for } P \text{ waves} \\
\frac{L}{\rho} &= \beta_V^2 \quad \text{for } SV \text{ waves} \\
\frac{N}{\rho} &= \beta_H^2 \quad \text{for } SH \text{ waves}
\end{aligned} \tag{1}
$$

and for vertical transmission:

$$
\begin{aligned}
\frac{C}{\rho} &= \alpha_V^2 \quad \text{for } P \text{ waves} \\
\frac{L}{\rho} &= \beta_V^2 \quad \text{for } S \text{ waves.}
\end{aligned} \tag{2}
$$

For the isotropic case, $A = C = \lambda + 2\mu$, $L = N = \mu$ and $F = \lambda$ (Love, 1927) where λ and μ are Lamé's constants. A cylindrical coordinate system (r, φ, z) is chosen with the origin on the free surface just above the source, with the z-axis taken positive downward.

We have rearranged Takeuchi and Saito's (1972) Eqs. 46 and 62, for SH and $P-SV$ cases, respectively, to obtain

$$
\begin{aligned}
\frac{df_1}{dz} &= -k f_2 + \frac{1}{L} f_4 \\
\frac{df_2}{dz} &= \frac{kF}{C} f_1 + \frac{1}{C} f_3 \\
\frac{df_3}{dz} &= -\omega^2 \rho f_2 + k f_4 \\
\frac{df_4}{dz} &= \left[k^2 \left(A - \frac{F^2}{C}\right) - \omega^2 \rho\right] f_1 - \frac{kF}{C} f_3 \\
\frac{df_5}{dz} &= \frac{1}{L} f_6 \\
\frac{df_6}{dz} &= (k^2 N - \omega^2 \rho) f_5
\end{aligned} \tag{3}
$$

where f_1, f_2 and f_5 are variables proportional to radial, vertical and transverse components of displacement and f_3, f_4 and f_6 are proportional to vertical, radial and tangential components of stress, respectively. k and ω represent horizontal wavenumber and angular frequency, respectively.

Equation (3) in matrix form

$$\frac{df}{dz} = \mathbf{Q}(\mathbf{z}) f(z) \tag{4}$$

is a system of n linear homogeneous ordinary differential equations for the functions $f_i(z)$, $i = 1, 2, \ldots, n$. Here $\mathbf{Q}(\mathbf{z})$ is a matrix representing material properties. An essential requirement of the propagator matrix method is that these properties are uniform within each layer (Gilbert and Backus, 1966). The solution of Eq. (4) is, using Sylvester's theorem,

$$
\begin{aligned}
f(z) &= e^{(z - z_0)\mathbf{Q}(\mathbf{z})} f(z_0) \\
&= a f(z_0)
\end{aligned} \tag{5}
$$

where z_0 is a reference depth. The function $e^{(z-z_0)\mathbf{Q}(\mathbf{z})} = a$ is called the matricant, matrizant or layer matrix for a homogeneous medium. Using the familiar $\mathbf{E}$ matrix (Haskell 1953, Harkrider 1964), the most general solution of Eq. (4) is

$$f = \mathbf{E} \Lambda \mathbf{K} \tag{6}$$

and

$$a = \mathbf{E} \Lambda \mathbf{E}^{-1} \tag{7}$$

where $\mathbf{E}$ is the eigenvector matrix of $\mathbf{Q}(\mathbf{z})$ (Appendix A), Λ is a diagonal matrix which explains the phase variation along the depth direction and consists of eigenvalues of $\mathbf{Q}(\mathbf{z})$, and $\mathbf{K}$ is a constant vector which consists of coefficients of both up-going and down-going waves. Expressions for these quantities are

$$\Lambda = \operatorname{diag}\left[e^{\nu_1 z}, e^{\nu_2 z}, e^{-\nu_1 z}, e^{-\nu_2 z}, e^{\nu_3 z}, e^{-\nu_3 z}\right] \tag{8}$$

where ν_1, ν_2 and ν_3 are eigenvalues of $\mathbf{Q}(\mathbf{z})$, and

$$\mathbf{K} = [\mathbf{A}'', \mathbf{B}'', \mathbf{A}', \mathbf{B}', \mathbf{C}'', \mathbf{C}']^{\mathbf{T}}. \tag{9}$$

In this expression $''$ refers to up-going waves and $'$ refers to down-going waves. ν_1 and ν_2 are roots of the equation

$$
\begin{aligned}
&\nu^4 - \left[\frac{k^2 A - \omega^2 \rho}{L} + \frac{k^2 L - \omega^2 \rho}{C} - \frac{k^2 (F+L)^2}{CL}\right] \nu^2 \\
&\quad + \frac{(k^2 L - \omega^2 \rho)(k^2 A - \omega^2 \rho)}{CL} = 0
\end{aligned} \tag{10}
$$

and ν_3 is obtained from

$$\nu_3^2 = \frac{N k^2 - \omega^2 \rho}{L}. \tag{11}$$

For the isotropic case, there are only two eigenvalues

$$
\begin{aligned}
\nu_\alpha^2 &= k^2 - \frac{\omega^2}{\alpha^2} \\
\nu_\beta^2 &= k^2 - \frac{\omega^2}{\beta^2}
\end{aligned} \tag{12}
$$

where α, β are P-, S-wave velocities respectively.

The derivation of the relation between surface displacements and wave coefficients in the half-space, in terms of $\mathbf{K}_N$ (N stands for half-space) is given for an isotropic medium by Wang and Herrmann (1980) and Wang (1981) as

$$\mathbf{K}_N = XS + R(f)_1 \tag{13}$$

where

$$
\begin{aligned}
X &= E_N^{-1} \alpha_{N-1} \ldots \alpha_m (d_m - h_m) \\
Z &= \alpha_m (h_m) \ldots \alpha_1 \\
R &= XZ = E_N^{-1} \alpha_{N-1} \ldots \alpha_1 .
\end{aligned} \tag{14}
$$

S is the source vector for a double-couple or explosion source (Appendix B) and $(f)_1$ is the surface value of f. d_m is the thickness of the m-th layer containing the source with depth h_m beneath the $m-1$ interface. At the free surface, stresses will vanish, yielding

$$(f)_1=[f_1, f_2, 0, 0, f_5, 0]^{\mathrm{T}}. \tag{15}$$

In the half-space, there are no up-going waves, so

$$\mathbf{K}_N=[0, 0, \mathbf{A}'_N, \mathbf{B}'_N, 0, \mathbf{C}'_N]^{\mathrm{T}}. \tag{16}$$

The function f on the free surface becomes

$$\begin{pmatrix} f_1 \\ f_2 \end{pmatrix}_1 = \frac{(-1)}{R|^{12}_{12}} \begin{bmatrix} R_{22} & -R_{12} \\ -R_{21} & R_{11} \end{bmatrix} \cdot \begin{bmatrix} X_{1i} & S_i \\ X_{2i} & S_i \end{bmatrix} \qquad i=1, \ldots, 4 \tag{17}$$

$$(f_5)_1=(-1)\frac{X_{5i}S_i}{R_{55}} \qquad i=5, 6. \tag{18}$$

For numerical accuracy in computation, relation (17) can be written as a compound matrix ($R|^{ij}_{kl}=R_{ik}R_{jl}-R_{il}R_{jk}$),

$$\begin{pmatrix} f_1 \\ f_2 \end{pmatrix}_1 = \frac{1}{R|^{12}_{12}} \begin{pmatrix} -S_i & X|^{12}_{ij} & Z_{j2} \\ S_i & X|^{12}_{ij} & Z_{j1} \end{pmatrix} \tag{19}$$

where from (14) and Dunkin (1965),

$$\begin{aligned} X|^{12}_{ij} &= E_N^{-1}|^{12}_{mn}\, a_{N-1}|^{mn}_{op} \ldots a_{m+1}|^{qr}_{st}\, a_m|^{st}_{ij} \\ R|^{12}_{12} &= E_N^{-1}|^{12}_{mn}\, a_{N-1}|^{mn}_{op} \ldots a_2|^{qr}_{st}\, a_1|^{st}_{12}. \end{aligned} \tag{20}$$

These matrices are listed in Appendix A. The advantages of using compound matrices have been discussed in several previous publications (Knopoff, 1964; Dunkin, 1965; Gilbert and Backus, 1966). We have found that the use of analytical expressions for compound matrices is more stable than element multiplication for computations.

Integral solution and times histories

For a point source, the free surface displacements are:

$$u_z(r, \varphi, 0, \omega) = \frac{1}{2\pi} \sum_{m=-\infty}^{\infty} \int_0^{\infty} Y_k^m(r, \varphi) f_2(\omega, k)\, k\, dk, \tag{19a}$$

$$u_r(r, \varphi, 0, \omega) = \frac{1}{2\pi} \sum_{m=-\infty}^{\infty} \int_0^{\infty} \left[\frac{\partial Y_k^m}{\partial r} f_1(\omega, k) + \frac{1}{r}\frac{\partial Y_k^m}{\partial \varphi} f_5(\omega, k)\right] dk, \tag{19b}$$

$$u_\varphi(r, \varphi, 0, \omega) = \frac{1}{2\pi} \sum_{m=-\infty}^{\infty} \int_0^{\infty} \left[\frac{1}{r}\frac{\partial Y_k^m}{\partial \varphi} f_1(\omega, k) - \frac{\partial Y_k^m}{\partial r} f_5(\omega, k)\right] dk \tag{19c}$$

where $Y_k^m(r, \varphi)=J_m(kr)\,e^{im\varphi}$ $m=0, \pm 1, \pm 2, \ldots$ (Takeuchi and Saito, 1972).

For a buried double-couple source without moment, with unit vector $\mathbf{n}=(n_1, n_2, n_3)$ normal to the fault and $v=(v_1, v_2, v_3)$ in the direction of the force (Haskell, 1963; Saito, 1967; Takeuchi and Saito, 1972), the Fourier transformed displacements at the free surface at a distance r from the origin (Wang and Herrmann, 1980; Herrmann and Wang, 1985) are

$$\begin{aligned} u_z(r, 0, \omega) &= ZSS[(v_1 n_1 - v_2 n_2)\cos 2\varphi + (v_1 n_2 + v_2 n_1)\sin 2\varphi] \\ &\quad + ZDS[(v_1 n_3 + v_3 n_1)\cos\varphi + (v_2 n_3 + v_3 n_2)\sin\varphi] \\ &\quad + ZDD[v_3 n_3], \end{aligned} \tag{20a}$$

$$\begin{aligned} u_r(r, 0, \omega) &= RSS[(v_1 n_1 - v_2 n_2)\cos 2\varphi + (v_1 n_2 + v_2 n_1)\sin 2\varphi] \\ &\quad + RDS[(v_1 n_3 + v_3 n_1)\cos\varphi + (v_2 n_3 + v_3 n_2)\sin\varphi] \\ &\quad + RDD[v_3 n_3], \end{aligned} \tag{20b}$$

$$\begin{aligned} u_\varphi(r, 0, \omega) &= TSS[(v_1 n_1 - v_2 n_2)\sin 2\varphi - (v_1 n_2 + v_2 n_1)\cos 2\varphi] \\ &\quad + TDS[(v_1 n_3 + v_3 n_1)\sin\varphi - (v_2 n_3 + v_3 n_2)\cos\varphi]. \end{aligned} \tag{20c}$$

In the notations *ZDD*, *ZDS*, *ZSS*, *RDD*, *RDS*, *RSS*, *TDS* and *TSS*, the first letter refers to component (*Z* - vertical, *R* - radial and *T* - tangential) and the last two letters refer to one of the three fundamental shear dislocations of Harkrider (1976). *DD* refers to 45° dip-slip, *DS* to 90° dip-slip and *SS* to pure strike-slip motion.

Integral representations of the displacement in the frequency domain in Eqs. 19 and 20 are summarized in general form as

$$I_m = \int_0^{\infty} F(k, \omega)\, J_m(kr)\, dk \qquad m=0, 1, 2 \tag{21}$$

where the kernel $F(k, \omega)$ (Appendix B) is a function of wavenumber, frequency, source depth and layer parameters. The wavenumber integration (21) can be evaluated by a discrete wavenumber summation described by Bouchon (1981). Yao and Harkrider (1983) discussed details of this technique. The wavenumber sample interval (dk) and total number of samples depend on the distance, frequency, the depth of the source and the layer parameters. To obtain a complete seismogram, the wavenumber summation method requires very dense wavenumber sampling. This requires extensive computation time and large amounts of computer memory. In order to efficiently use time and space, sampling may be optimized with the distance of computation, frequency, layer parameters and depth of the source. Some criteria for deciding on the wavenumber sampling interval (dk) had been discussed by Bouchon (1981).

To avoid the influence of singularities of the kernel $F(k, \omega)$, two techniques can be used (Bouchon, 1981). Frequency can be made complex or attenuation can be introduced into the computations to make the velocities complex. In the present study, we have chosen the first technique. We later remove the imaginary part of the frequency (damping factor) from the time-domain solution.

The time-domain response, in general is

$$u(t) = \int_{-\infty}^{\infty} S(\omega)\, u(\omega)\, e^{i\omega t}\, d\omega \tag{22}$$

where $S(\omega)$ is the frequency-domain response of the source-time function. In our test cases we have used a

1
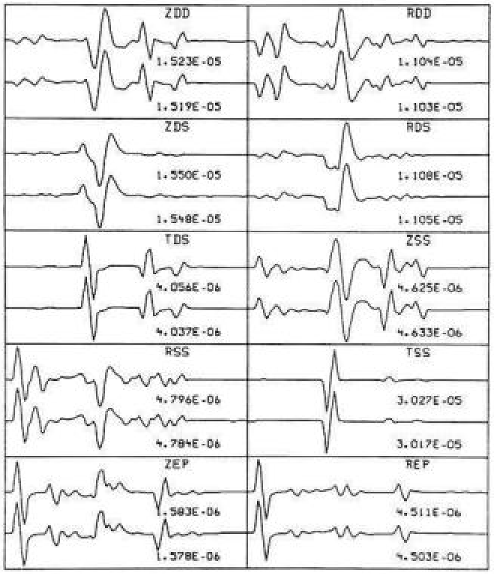

2
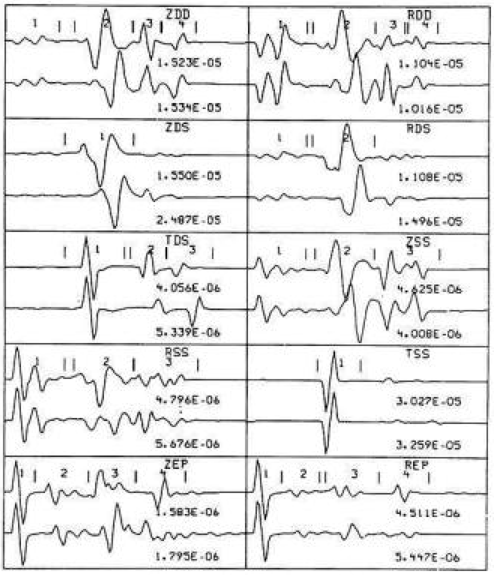

Fig. 1. Synthetic seismograms at a distance of 75 km, for a source at a depth of 10 km, using present computations (*upper trace*) and results of Herrmann and Wang (1985) (*lower trace*). Ground velocity is computed over a time interval between 11.30 and 43.05 s. The numerical value adjacent to each trace is the peak ground velocity in units of cm/s. EP refers to an explosion source. Both seismograms are computed for the isotropic model given in Table 1

Fig. 2. Synthetic seismograms at a distance of 75 km, for a source at a depth of 10 km, using methods of this study for an isotropic model (*upper trace*) and an anisotropic model (*lower trace*). Ground velocity is computed over a time interval between 11.30 and 43.05 s

Table 1. Layer parameters for the test models

d (km)	α_H (km/s)	α_V (km/s)	β_V (km/s)	β_H (km/s)	η (km/s)	ρ (gm/cm^3)
Isotropic simple crustal models						
40	6.15	6.15	3.55	3.55	3.552	2.8
	8.09	8.09	4.67	4.67	4.6723	3.3
Anisotropic simple crustal model						
40	6.15	5.8425	3.195	3.55	3.525	2.8
	8.09	8.09	4.67	4.67	4.6723	3.3

where $\eta=\sqrt{\frac{F}{\rho}}$.

parabolic pulse (Herrmann, 1979) as a source-time function.

We used the simple crustal model in Table 1 for testing the program with an isotropic model. This model was used by Herrmann and Wang (1985) and allows us to compare our computational results with those of other methods. The velocity response at a distance of 75 km for a source depth of 10 km and sampling interval of 0.25 s, using present computations (upper trace), are compared with results of Hermann and Wang (1985) (lower trace) in Fig. 1. This comparison shows that our new algorithm provides results which are consistent with other methods for a model with isotropic elastic parameters ($A=C=\lambda+2\mu$, $L=N=\mu$ and $F=\lambda$).

Numerical examples for anisotropic medium

We alter the isotropic crustal model in Table 1 to obtain an anisotropic model on which to perform numerical tests. For the anisotropic model, the velocity of the vertically traveling P wave is decreased by 5 % and that of the vertically traveling S wave is decreased by 10 % compared to the velocities in the isotropic model. The synthetics obtained for this model are compared to

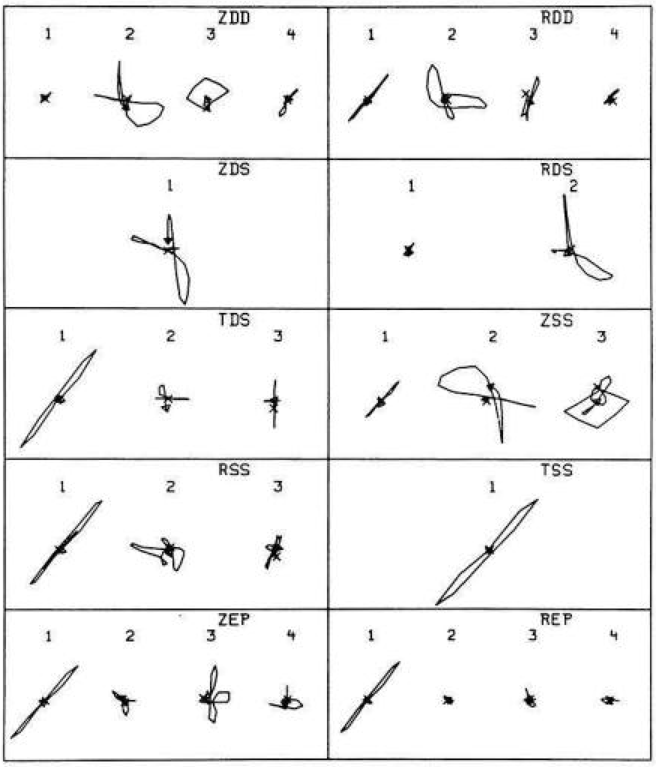

Fig. 3. Particle motion diagrams for different time windows of seismograms in Fig. 2

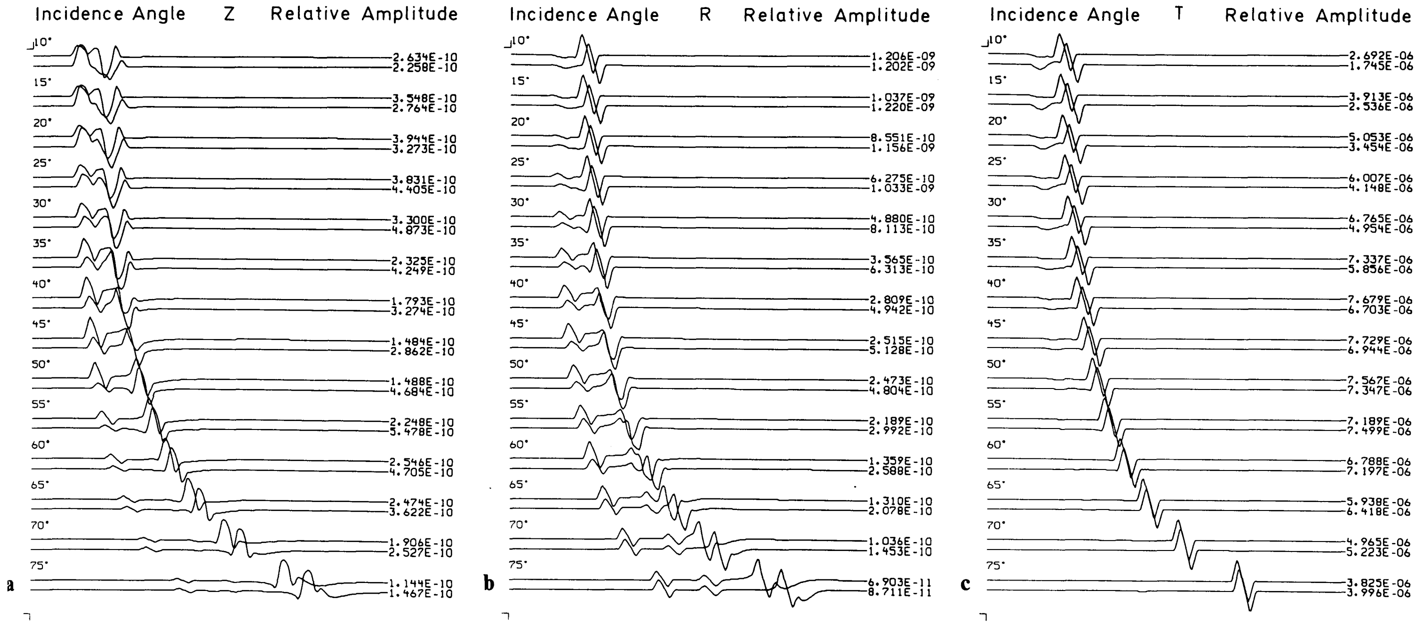

Fig. 4. **a** Vertical-component seismograms at different incidence angles for an isotropic half-space (*upper trace*) and an anisotropic half-space (*lower trace*) from a source buried at a depth of 40 km. A pure vertical strike-slip focal mechanism is used. The duration of each seismogram is 64 s with sampling interval of 0.25 s. The seismograms were recorded at an azimuth of 0° from the strike direction of the source. **b** Radial-component seismograms for the same model and source as those described in Fig. 4a. **c** Transverse-component seismograms for the same model and source as those described in Fig. 4a

those for the isotropic case in Fig. 2. As in Fig. 1, they pertain to a distance of 75 km, a source depth of 10 km and a sampling interval of 0.25 s. The seismograms are plotted adjacent to one another for easy comparison, the upper trace pertaining to the isotropic case and lower trace to the anisotropic case. Notable differences occur in the amplitudes and phases between each pair of seismograms. In the transverse components (*TDS* and *TSS*), the primary *S* phases arrive at the same time because the wave at this distance is traveling nearly horizontally, so the *S*-wave velocity is nearly identical for both the isotropic and anisotropic case. Later phases arrive at different times because of splitting of the shear waves. Interesting phases are observed on the vertical (*ZDD*, *ZDS*, *ZSS*, *ZEP*) and radial (*RDD*, *RDS*, *RSS*, *REP*) components. At this distance the *S* wave arrives later for the anisotropic model and the shape of the seismogram differs from that for the isotropic model.

Figure 3 shows the particle motion for the different time windows in Fig. 2. The horizontal axis represents motion for the isotropic model and the vertical axis for the anisotropic model. From the particle motion plot, we see that the motion for the *P* phases is almost the same even though the velocity variation is 5%. For the vertical and radial components, the *S* and Rayleigh wave portions of the seismograms (window 2 for *ZDD*, *RDD*, *RDS*, *ZSS* and window 1 for *ZDS* in Figs. 2 and 3) for the isotropic case lead those for the anisotropic case by more than 90°. Notable difference also occur in the amplitudes and times of the later arrivals.

In a general anisotropic medium, the energy traveling in the group-velocity direction does not necessary coincide with the phase-velocity direction (Crampin, 1981). This deviation depends on the type of symmetry in the medium, the type of wave and the propagation direction of the wave. Polarization angles of the various waves give some idea of the nature of the anisotropy, provided that the source or other effects do not cause anomalous particle motion in the observed seismograms.

In a transversely isotropic medium, fundamental-mode waves travel along their phase-velocity direction, but compressional waves are not, in general, parallel to, nor are the shear waves perpendicular to, the phase-velocity direction. For a vertical axis of symmetry, the phase velocity varies with incidence angle. To illustrate the different phenomena in transversely isotropic media, we have computed individual synthetic seismograms at different incidence angles for a pure strike-slip dislocation source in both an isotropic medium and an anisotropic medium. Both models consist of a semi-infinite half-space with the parameters of the upper layer of the model in Table 1. The incidence angle is measured from the downward normal to the surface. Seismograms were computed at 14 different distances with an interval in incidence angle of 5°. All computations were for an azimuth of 0° from a source with a depth of 40 km. With this configuration, both vertically and horizontally polarized shear waves will be present. The seismograms are shown in Fig. 4a–c for vertical, radial and transverse components, respectively. In these figures, the upper trace pertains to the isotropic model and the lower trace to the anisotropic model. For the vertical and radial components, the shear wave is an *SV* wave and for the transverse component it is an *SH* wave. From the figures, *SV* waves in the anisotropic medium appear later than those in the isotropic medium when the wave propagates vertically and horizontally. For the transverse component, the *SH* wave in the anisotropic model arrives substantially later than that in the isotropic model at short distances but comes closer and closer to it as the waves travel more horizontally at larger distances. This phenomenon was observed in near surface shale by Robertson and Corrigan (1983) and has been explained by Crampin (1981) and Peacock and Crampin (1985).

Conclusions

We have developed a method to compute complete synthetic seismograms, including all body and surface waves, generated in a transversely isotropic medium by a dislocation or explosion source. These seismograms can include very high frequencies, thus making it possible to study regional phases in various frequency bands. To obtain a complete seismogram, the wavenumber summation method requires very dense wavenumber sampling. This requires extensive computation time and large amounts of computer memory. In order to efficiently use time and space, sampling may be optimized with the distance of computation, frequency, layer parameters and depth of the source. We have performed these computations using propagator matrices and the discrete wavenumber summation method and have verified the algorithm by comparing results for a simple crustal model with results observed using other isotropic methods. A comparison of time histories of the wave motion for a transversely isotropic model with that predicted for an isotropic model shows that amplitudes and wave forms of both body and surface waves, as well as travel times, can be markedly altered by the presence of anisotropy.

Appendix A: Layer matrices for transversely isotropic media

Notation

ρ=density; ω=frequency; k=wavenumber; v_i, $i=1,2,3$ are eigenvalues as defined in the main text.

$$\gamma_i=\frac{k v_i(F+L)}{\omega^2\rho-k^2L+v_i^2C},$$

$$X_i=Cv_i\gamma_i-kF,$$

$$Y_i=L(v_i+k\gamma_i),$$

$i=1,2$ for P-SV case.

$$\mathbf{a}=\frac{1}{X_2-X_1},$$

$$\mathbf{b}=\frac{1}{Y_1\gamma_2-Y_2\gamma_1},$$

$$P=v_1z;\quad Q=v_2z,$$

$$CP=\cosh P;\quad CQ=\cosh Q,$$

$$SP=\sinh P;\quad SQ=\sinh Q.$$

E matrix:

$$\mathbf{E}=\begin{bmatrix}1&1&1&1&0&0\\ \gamma_1&\gamma_2&-\gamma_1&-\gamma_2&0&0\\ X_1&X_2&X_1&X_2&0&0\\ Y_1&Y_2&-Y_1&-Y_2&0&0\\ 0&0&0&0&1&1\\ 0&0&0&0&Lv_3&-Lv_3\end{bmatrix}$$

$\mathbf{E}^{-1}$ matrix:

$$\mathbf{E}^{-1}=\frac{1}{2}\begin{bmatrix}\mathbf{a}X_2&-\mathbf{b}Y_2&-\mathbf{a}&\mathbf{b}\gamma_2&0&0\\ -\mathbf{a}X_1&\mathbf{b}Y_1&\mathbf{a}&-\mathbf{b}\gamma_1&0&0\\ \mathbf{a}X_2&\mathbf{b}Y_2&-\mathbf{a}&-\mathbf{b}\gamma_2&0&0\\ -\mathbf{a}X_1&-\mathbf{b}Y_1&\mathbf{a}&\mathbf{b}\gamma_1&0&0\\ 0&0&0&0&1&\frac{1}{Lv_3}\\ 0&0&0&0&1&-\frac{1}{Lv_3}\end{bmatrix}$$

a matrix: $\mathbf{E}\Lambda\mathbf{E}^{-1}$

$$a_{11}=\mathbf{a}(X_2CP-X_1CQ)$$
$$a_{12}=\mathbf{b}(Y_1SQ-Y_2SP)$$
$$a_{13}=\mathbf{a}(CQ-CP)$$
$$a_{14}=\mathbf{b}(\gamma_2SP-\gamma_1SQ)$$
$$a_{21}=\mathbf{a}(X_2\gamma_1SP-X_1\gamma_2SQ)$$
$$a_{22}=\mathbf{b}(Y_1\gamma_2CQ-Y_2\gamma_1CP)$$
$$a_{23}=\mathbf{a}(\gamma_2SQ-\gamma_1SP)$$
$$a_{24}=\mathbf{b}\gamma_1\gamma_2(CP-CQ)$$
$$a_{31}=\mathbf{a}X_1X_2(CP-CQ)$$
$$a_{32}=\mathbf{b}(X_2Y_1SQ-X_1Y_2SP)$$
$$a_{33}=\mathbf{a}(X_2CQ-X_1CP)$$
$$a_{34}=\mathbf{b}(X_1\gamma_2SP-X_2\gamma_1SQ)$$
$$a_{41}=\mathbf{a}(X_2Y_1SP-X_1Y_2SQ)$$
$$a_{42}=\mathbf{b}Y_1Y_2(CQ-CP)$$
$$a_{43}=\mathbf{a}(Y_2SQ-Y_1SP)$$
$$a_{44}=\mathbf{b}(Y_1\gamma_2CP-Y_2\gamma_1CQ)$$
$$a_{55}=\cosh v_3z$$
$$a_{56}=\frac{1}{Lv_3}\sinh v_3z$$
$$a_{65}=Lv_3\sinh v_3z$$
$$a_{66}=\cosh v_3z$$

Compound layer matrix:

$$a|_{12}^{12}=a|_{34}^{34}=\mathbf{a}\mathbf{b}[(X_1Y_2\gamma_1+X_2Y_1\gamma_2)CPCQ\\ -(X_1Y_1\gamma_2+X_2Y_2\gamma_1)\\ -(X_1Y_2\gamma_2+X_2Y_1\gamma_1)SPSQ]$$
$$a|_{13}^{12}=a|_{34}^{24}=\mathbf{a}[\gamma_2CPSQ-\gamma_1CQSP]$$
$$a|_{14}^{12}=a|_{34}^{23}=\mathbf{a}\mathbf{b}[\gamma_1\gamma_2(X_2+X_1)(1-CPCQ)\\ +(X_2\gamma_1^2+X_1\gamma_2^2)SPSQ]$$
$$a|_{23}^{12}=a|_{34}^{14}=\mathbf{a}\mathbf{b}[(Y_1\gamma_2+Y_2\gamma_1)(CPCQ-1)\\ -(Y_1\gamma_1+Y_2\gamma_2)SPSQ]$$
$$a|_{24}^{12}=a|_{34}^{13}=\mathbf{b}[\gamma_1CPSQ-\gamma_2CQSP]$$
$$a|_{34}^{12}=\mathbf{a}\mathbf{b}[2\gamma_1\gamma_2(CPCQ-1)-(\gamma_1^2+\gamma_2^2)SPSQ]$$
$$a|_{12}^{13}=a|_{24}^{34}=\mathbf{b}[X_2Y_1CPSQ-X_1Y_2CQSP]$$
$$a|_{13}^{13}=a|_{24}^{24}=CPCQ$$
$$a|_{14}^{13}=a|_{24}^{23}=\mathbf{b}[X_1\gamma_2CQSP-X_2\gamma_1CPSQ]$$
$$a|_{23}^{13}=a|_{24}^{14}=\mathbf{b}[Y_1CPSQ-Y_2CQSP]$$
$$a|_{24}^{13}=-\frac{\mathbf{b}}{\mathbf{a}}SPSQ$$

$$a|_{12}^{14}=a|_{23}^{34}=\mathbf{a}\mathbf{b}[Y_1 Y_2(X_1+X_2)(CPCQ-1) -(X_1 Y_2^2+X_2 Y_1^2)SPSQ]$$

$$a|_{13}^{14}=a|_{23}^{24}=\mathbf{a}[Y_2\, CPSQ-Y_1\, CQSP]$$

$$a|_{14}^{14}=a|_{23}^{23}=\mathbf{a}\mathbf{b}[(X_2 Y_1\gamma_2+X_1 Y_2\gamma_1) -(X_1 Y_1\gamma_2+X_2 Y_2\gamma_1)CPCQ +(X_1 Y_2\gamma_2+X_2 Y_1\gamma_1)SPSQ]$$

$$a|_{23}^{14}=\mathbf{a}\mathbf{b}[2Y_1 Y_2(CPCQ-1)-(Y_1^2+Y_2^2)SPSQ]$$

$$a|_{12}^{23}=a|_{14}^{34}=\mathbf{a}\mathbf{b}[X_1 X_2(Y_1\gamma_2+Y_2\gamma_1)(1-CPCQ) +(X_2^2 Y_1\gamma_1+X_1^2 Y_2\gamma_2)SPSQ]$$

$$a|_{13}^{23}=a|_{14}^{24}=\mathbf{a}[X_2\gamma_1\, CQSP-X_1\gamma_2\, CPSQ]$$

$$a|_{14}^{23}=\mathbf{a}\mathbf{b}[2X_1 X_2\gamma_1\gamma_2(CPCQ-1)-(X_1^2\gamma_2^2+X_2^2\gamma_1^2)SPSQ]$$

$$a|_{12}^{24}=a|_{13}^{34}=\mathbf{a}[X_1 Y_2\, CPSQ-X_2 Y_1\, CQSP]$$

$$a|_{13}^{24}=-\frac{\mathbf{a}}{\mathbf{b}}SPSQ$$

$$a|_{12}^{34}=\mathbf{a}\mathbf{b}[2X_1 X_2 Y_1 Y_2(CPCQ-1)-(X_1^2 Y_1^2+Y_1^2 Y_2^2)SPSQ]$$

$\mathbf{E}^{-1}|_{ij}^{12}$ matrix

$$E^{-1}|_{12}^{12}=\frac{1}{4}\mathbf{a}\mathbf{b}(X_2 Y_1-X_1 Y_2)$$

$$E^{-1}|_{13}^{12}=\frac{\mathbf{a}}{4}$$

$$E^{-1}|_{14}^{12}=\frac{\mathbf{a}\mathbf{b}}{4}(X_1\gamma_2-X_2\gamma_1)$$

$$E^{-1}|_{23}^{12}=\frac{\mathbf{a}\mathbf{b}}{4}(Y_1-Y_2)$$

$$E^{-1}|_{24}^{12}=-\frac{\mathbf{b}}{4}$$

$$E^{-1}|_{34}^{12}=\frac{\mathbf{a}\mathbf{b}}{4}(\gamma_1-\gamma_2)$$

Appendix B

Integrals: I

$$ZDD=\int_0^\infty F_1(k,\omega)J_0(kr)k\,dk$$

$$RDD=-\int_0^\infty F_2(k,\omega)J_1(kr)k\,dk$$

$$ZDS=\int_0^\infty F_3(k,\omega)J_1(kr)k\,dk$$

$$RDS=\int_0^\infty F_4(k,\omega)J_0(kr)k\,dk -\frac{1}{r}\int_0^\infty [F_4(k,\omega)+F_9(k,\omega)]J_1(kr)\,dk$$

$$TDS=\int_0^\infty F_9(k,\omega)J_0(kr)k\,dk -\frac{1}{r}\int_0^\infty [F_4(k,\omega)+F_9(k,\omega)]J_1(kr)\,dk$$

$$ZSS=\int_0^\infty F_5(k,\omega)J_2(kr)k\,dk$$

$$RSS=\int_0^\infty F_6(k,\omega)J_1(kr)k\,dk -\frac{2}{r}\int_0^\infty [F_6(k,\omega)+F_{10}(k,\omega)]J_2(kr)\,dk$$

$$TSS=\int_0^\infty F_{10}(k,\omega)J_1(kr)k\,dk -\frac{2}{r}\int_0^\infty [F_6(k,\omega)+F_{10}(k,\omega)]J_2(kr)\,dk$$

$$ZEP=\int_0^\infty F_7(k,\omega)J_0(kr)k\,dk$$

$$REP=-\int_0^\infty F_8(k,\omega)J_1(kr)k\,dk$$

Kernels: $F_i(k,\omega)$

$$F_1(k,\omega)=\frac{1}{R|_{12}^{12}}[S_2^0(-X|_{12}^{12}Z_{11}+X|_{23}^{12}Z_{31}+X|_{24}^{12}Z_{41}) +S_4^0(X|_{14}^{12}Z_{11}+X|_{24}^{12}Z_{21}+X|_{34}^{12}Z_{31})]$$

$$F_2(k,\omega)=\frac{1}{R|_{12}^{12}}[S_2^0(-X|_{12}^{12}Z_{12}+X|_{23}^{12}Z_{32}+X|_{24}^{12}Z_{42}) +S_4^0(X|_{14}^{12}Z_{12}+X|_{24}^{12}Z_{22}+X|_{34}^{12}Z_{32})]$$

$$F_3(k,\omega)=\frac{S_1^1}{R|_{12}^{12}}[X|_{12}^{12}Z_{21}+X|_{13}^{12}Z_{31}+X|_{14}^{12}Z_{41}]$$

$$F_4(k,\omega)=-\frac{S_1^1}{R|_{12}^{12}}[X|_{12}^{12}Z_{22}+X|_{13}^{12}Z_{32}+X|_{14}^{12}Z_{42}]$$

$$F_5(k,\omega)=-\frac{S_4^2}{R|_{12}^{12}}[X|_{14}^{12}Z_{11}+X|_{24}^{12}Z_{21}+X|_{34}^{12}Z_{31}]$$

$$F_6(k,\omega)=\frac{S_4^2}{R|_{12}^{12}}[X|_{14}^{12}Z_{12}+X|_{24}^{12}Z_{22}+X|_{34}^{12}Z_{32}]$$

$$F_7(k,\omega)=\frac{1}{R|_{12}^{12}}[S_2^E(-X|_{12}^{12}Z_{11}+X|_{23}^{12}Z_{31}+X|_{24}^{12}Z_{41}) +S_4^E(X|_{14}^{12}Z_{11}+X|_{24}^{12}Z_{21}+X|_{34}^{12}Z_{31})]$$

$$F_8(k,\omega)=\frac{1}{R|_{12}^{12}}[S_2^E(-X|_{12}^{12}Z_{12}+X|_{23}^{12}Z_{32}+X|_{24}^{12}Z_{42}) +S_4^E(X|_{14}^{12}Z_{12}+X|_{24}^{12}Z_{22}+X|_{34}^{12}Z_{32})]$$

$$F_9(k,\omega)=-\frac{S_5^1 X_{55}}{R_{55}}$$

$$F_{10}(k,\omega)=-\frac{S_6^1 X_{56}}{R_{55}}$$

Source matrices: S^m, $m=0,1,2$

Dislocation source

$$S^0=M_0(\omega)\begin{bmatrix}0\\ \frac{1}{C}\\ 0\\ -\frac{k}{2}\left(1+\frac{2F}{C}\right)\\ 0\\ 0\end{bmatrix}\quad \text{for } 45^\circ \text{ dip-slip.}$$

$$S^1=M_0(\omega)\begin{bmatrix}\frac{i}{2L}\\ 0\\ 0\\ 0\\ \frac{1}{2L}\\ 0\end{bmatrix}\quad \text{for vertical dip-slip.}$$

$$S^2 = M_0(\omega) \begin{bmatrix} 0 \\ 0 \\ 0 \\ \frac{ik}{2} \\ 0 \\ \frac{k}{2} \end{bmatrix} \quad \text{for vertical strike-slip.}$$

Here $M_0(\omega)$ is the seismic moment.

Explosion source

$$S^E = M_0(\omega) \begin{bmatrix} 0 \\ \frac{1}{C} \\ 0 \\ k\left(1-\frac{F}{C}\right) \end{bmatrix}$$

Acknowledgements. The authors wish to thank Dr. Robert B. Herrmann for discussion of numerical problems during these computations. We would also like to thank Drs. C.Y. Wang and C.K. Saikia for helpful discussions. This research was supported by the Advanced Research Projects Agency of the Department of Defense and was monitored by the Air Force Geophysics Laboratory under Contract F19628-85-k-0021.

References

Alterman, Z., Jarosch, H., Pekeris, C.L.: Oscillations of the earth. Proc. Roy. Soc. Ser. A **252**, 80–95, 1959

Anderson, D.L.: Elastic wave propagation in layered anisotropic media. J. Geophys. Res. **66**, 2953–2963, 1961

Anderson, D.L., Dziewonski, A.M.: Upper mantle anisotropy: evidence from free oscillations. Geophys. J. R. Astron. Soc. **69**, 383–404, 1982

Bamford, D., Crampin, S.: Seismic anisotropy – the state of the art. Geophys. J. R. Astron. Soc. **49**, 1–8, 1977

Bezgodkov, V.A., Yegorkina, G.V.: Experimental study of the anisotropy of longitudinal and transverse waves from local earthquake records. Geophys. J. R. Astron. Soc. **76**, 179–189, 1984

Booth, D.C., Crampin, S.: The anisotropic reflectivity technique theory. Geophys. J. R. Astron. Soc. **72**, 755–766, 1983

Bouchon, M.: A simple method to calculate Green's functions for elastic layered media. Bull. Seismol. Soc. Amer. **73**, 959-971, 1981

Cara, M., Nercessian, A., Nolet, G.: New inferences from higher mode data in western Europe and northern Eurasia. Geophys. J. R. Astron. Soc. **61**, 459–478, 1980

Crampin, S.: The dispersion of surface waves in multilayered anisotropic media. Geophys. J. R. Astron. Soc. **21**, 387–402, 1970

Crampin, S.: A review of wave motion in anisotropic and cracked elastic-media. Wave Motion **3**, North-Holland Publishing Company, 343–391, 1981

Crampin, S., Taylor, D.B.: The propagation of surface waves in anisotropic media. Geophys. J. R. Astron. Soc. **25**, 71–87, 1971

Dunkin, J.W.: Computation of modal solutions in layered, elastic media at high frequencies. Bull. Seismol. Soc. Amer. **55**, 335–358, 1965

Fryer, G.J., Frazer, L.N.: Seismic waves in stratified anisotropic media, elastic media at high frequencies. Geophys. J. R. Astron. Soc. **78**, 691–710, 1984

Gilbert, F., Backus, G.E.: Propagator matrices in elastic wave and vibration problems. Geophysics **31**, 326–332, 1966

Harkrider, D.G.: Surface waves in multi-layered elastic media I: Rayleigh and Love waves from buried sources in a multilayered half space. Bull. Seismol. Soc. Amer. **54**, 627–679, 1964

Harkrider, D.G.: Potentials and displacements for two theoretical seismic sources. Geophys. J. R. Astron. Soc. **47**, 97–133, 1976

Harkrider, D.G., Anderson, D.L.: Computation of surface wave dispersion for multilayered anisotropic media. Bull. Seismol. Soc. Amer. **52**, 321–332, 1962

Haskell, N.A.: The dispersion of surface wave on multilayered media. Bull. Seismol. Soc. Amer. **43**, 17–34, 1953

Haskell, N.A.: Radiation pattern of Rayleigh waves from a fault of arbitrary dip and direction of motion in a homogeneous medium. Bull. Seismol. Soc. Amer. **53**, 619–642, 1963

Herrmann, R.B.: *SH*-wave generation by dislocation sources-*A* numerical study. Bull. Seismol. Soc. Amer. **69**, 1–15, 1979

Herrmann, R.B., Wang, C.Y.: A comparison of synthetic seismograms. Bull. Seismol. Soc. Amer. **75**, 41–56, 1985

Hess, H.H.: Seismic anisotropy of the uppermost mantle under oceans. Nature **203**, 629–631, 1964

Keith, C.M., Crampin, S.: Seismic body waves in anisotropic media: synthetic seismograms. Geophys. J. R. Astron. Soc. **49**, 225–243, 1977

Kennett, B.L.N.: Reflections, ray, and reverberations. Bull. Seismol. Soc. Amer. **64**, 1685–1696, 1974

Knopoff, L.: A matrix method for elastic wave problems. Bull. Seismol. Soc. Amer. **54**, 431–438, 1964

Kogan, S.D.: The azimuthal variation of teleseismic *P*-wave travel times. Geophys. J. R. Astron. Soc. **76**, 201–207, 1984

Love, A.E.H.: The mathematical theory of elasticity. London and New York: Cambridge Univ. Press 1927

Matuzawa, T.: Elastische Wellen in einem anisotropen Medium. Bull. Earthq. Res. Inst. Tokyo **21**, 231–234, 1943

Peacock, S., Crampin, S.: Shear-wave vibrator signals in transversely isotropic shale. Geophysics **52**, 1285–1293, 1985

Robertson, J.D., Corrigan, D.: Radiation patterns of a shear-wave vibrator in near-surface shale. Geophysics **48**, 19–26, 1983

Saito, M.: Excitation of free oscillations and surface waves by a point source in a vertically heterogeneous earth. J. Geophys. Res. **72**, 3689–3699, 1967

Schule, J.W., Knopoff, L.: Shear-wave polarization anisotropy in the Pacific Basin. Geophys. J. R. Astron. Soc. **49**, 145–165, 1977

Takeuchi, H., Saito, M.: Seismic surface waves. Methods in computational physics. Academic Press, New York, **11**, 217–295, 1972

Tanimoto, T., Anderson, D.L.: Mapping convection in the mantle. Geophys. Res. Lett. **11**, 287–290, 1984

Wang, C.Y.: Wave theory for seismogram synthesis. Ph. D. Dissertation, Saint Louis University, St. Louis, Missouri, 1981

Wang, C.Y., Herrmann, R.B.: A numerical study of *P*-, *SV*-, and *SH*-wave generation in a plane layered medium. Bull. Seismol. Soc. Amer. **70**, 1015–1036, 1980

Yao, Z.X., Harkrider, D.G.: A generalized reflection-transmission coefficient matrix and discrete wavenumber method for synthetic seismograms. Bull. Seismol. Soc. Amer. **73**, 1685–1699, 1983

Yu, G.K., Mitchell, B.J.: Regionalized shear velocity models of the Pacific upper mantle from observed Love and Rayleigh wave dispersion. Geophys. J.R. Astron. Soc. **57**, 311–341, 1979

Received December 6, 1985; revised version April 11, 1986
Accepted April 14, 1986